Published in final edited form as:
Neuroimage. 2010 January 1; 49(1): 240–248. doi:10.1016/j.neuroimage.2009.08.035.

FDDNP Binding Using MR Derived Cortical Surface Maps

HD Protas[1,2], **S-C Huang**[2], **V Kepe**[2], **K Hayashi**[3], **A Klunder**[3], **MN Braskie**[3,4], **L Ercoli**[5], **S. Bookheimer**[4,5,7], **PM Thompson**[3], **GW Small**[5,6], and **JR Barrio**[2]

[1] Department of Biomathematics, David Geffen School of Medicine at UCLA, CA 90095, USA

[2] Department of Molecular and Medical Pharmacology, David Geffen School of Medicine at UCLA, CA 90095, USA

[3] Laboratory of NeuroImaging, Department of Neurology, David Geffen School of Medicine at UCLA, CA 90095, USA

[4] Ahmanson-Lovelace Brain Mapping Center, David Geffen School of Medicine at UCLA, CA 90095, USA

[5] Department of Psychiatry and Biobehavioral Sciences, David Geffen School of Medicine at UCLA, CA 90095, USA

[6] Center on Aging, David Geffen School of Medicine at UCLA, CA 90095, USA

[7] Department of Psychology, David Geffen School of Medicine at UCLA, CA 90095, USA

Abstract

Objectives—To assess quantitatively the cortical pattern profile of regional FDDNP binding to beta-amyloid and neurofibrillary tangles on MR derived cortical maps, FDDNP PET images were corrected for movement and partial volume (PV), and optimized for kernel size. 3

Methods—FDDNP DVR PET images from 23 subjects (7 with Alzheimer's disease (AD), 6 with mild cognitive impairment and 10 controls) were obtained from Logan analysis using cerebellum as reference. A hemispheric cortical surface model for each subject was extracted from the MRI. The same transformations were applied to the FDDNP DVR PET images to map them into the same space. The cortical map with PV correction was calculated as the ratio of the DVR cortical surface and that of the simulated map, created from the mask derived from MRI and smoothed to the PET resolution. Discriminant analysis was used to order the FDDNP DVR cortical surfaces based on subjects' disease state. Linear regression was used to assess the rate of change of DVR vs. MMSE for each hemispheric cortical surface point.

Corresponding Author: Hillary Protas, Department of Molecular and Medical Pharmacology, David Geffen School of Medicine at UCLA B2-086 CHS, 10833 Le Conte Ave, Los Angeles, CA 90095, USA.

Financial Disclosure: The University of California, Los Angeles, owns a U.S. patent (6,274,119) entitled "Methods for Labeling β-Amyloid Plaques and Neurofibrillary Tangles," that uses the approach outlined in this article has been licensed to Siemens. Drs. Small, Huang, and Barrio are among the inventors, have received royalties, and may receive royalties on future sales. Dr. Small reports having served as a consultant and/or having received lecture fees from Abbott, Brainstorming Co., Dakim, Eisai, Forest, Medivation, Myriad Genetics, Novartis, Ortho-McNeil, Pfizer, Radica, and Siemens. Dr. Small also reports having received stock options from Dakim. Dr. Huang reports having received lecture fees from GlaxoSmithKline. Dr. Barrio reports having served as a consultant and having received lecture fees from Nihon Medi-Physics Co, Bristol-Meyer Squibb, PETNet Pharmaceuticals, and Siemens. Drs. Braskie, Ercoli, Protas, Kepe, Miller, Thompson, Klunder, and Bookheimer have no financial conflicts of interest.

Results—The FDDNP DVR cortical surface corrected for movement and PV had less hemispheric asymmetry. Optimal kernel size was determined to be 9mm. The corrected cortical surface map of FDDNP DVR showed clear spatial pattern that was consistent with the known pathological progression of AD.

Conclusion—Correcting for movement, PV as well as optimizing kernel size provide sensitive statistical analysis of FDDNP distribution which confirms in the living brain known pathology patterns earlier observed with cognitive decline with brain specimens.

Index Terms

cortical surface maps; MR; FDDNP PET

I. INTRODUCTION

Cortical surface maps have been used in functional Magnetic Resonance Imaging (fMRI) as well as Magnetic Resonance Imaging (MRI). Studies in the assessment of functional activity and structure on the entire cortical surface (Fischl and Dale, 2000; Rasser et al., 2005; Thompson et al., 2003; Van Essen and Drury, 1997) and cortical surface methods have also been adapted to Positron Emission Tomography (PET) analysis for molecular imaging probes such as 2-deoxy-2-[F-18]fluoro-D-glucose (FDG) (Loats et al., 1990; Park et al., 2006; Protas et al., 2005). MR cortical maps have been applied to 2-(1-{6-[(2-[F-18]Fluoroethyl)(methyl) amino]-2-naphthyl}ethylidene)malononitrile (FDDNP)) (Agdeppa et al., 2001; Guo and Zhang, 2007; Shin et al., 2008; Small et al., 2006) PET, which provides detailed visualization (Braskie et al., 2008) of the pattern of beta-amyloid plaques (Aβ) and neurofibrillary tangles (NFT) in the living brain of progressive Alzheimer's disease(AD). This distribution has striking similarities to the one demonstrated by post mortem analysis of Aβ and NFT in human brain specimens in AD (Braak and Braak, 1991, 1997) and cortical thinning with disease progression observed with MRI (Thompson et al., 2003). In this work, three methodological variables, namely head movement, kernel size and partial volume correction were carefully investigated with the intent to produce statistical optimization of FDDNP PET cortical binding maps. In the previous study (Braskie et al., 2008), kernel of 7 mm was used without optimization. Movement correction and partial volume correction were not available at that time. Low cortical FDDNP signals are significantly enhanced by optimization of these methodological variables which provide a more accurate quantitative cortical distribution of FDDNP binding on the cortical surface map in the various stages of disease progression (e.g., control subjects at risk, mild cognitive impairment (MCI) and early AD).

II. MATERIALS AND METHODS

A. Subjects

Seven AD (76±10 years, 4/3 Female/Male), 6 MCI (73±13 years, 4/2 Female/Male) and 10 control (71±10 years, 7/3 Female/Male) subjects were part of this work. All subjects were part of a large study group (Small et al., 2006). Two sets of criteria were used for subject selection: First, inclusion of subjects to cover the disease spectra with bias for subjects with very early disease (MCI and control subjects at risk); and also subjects with available T1 MRI scans performed in close proximity to the PET scans within 6 months. Subjects with a history of stroke, head injury, or any disease other than AD that would confound cognition were excluded. This study was approved by the Institutional Review Board of University of California, Los Angeles and all subjects themselves or through medical proxies gave informed written consent. AD and MCI subjects met diagnostic standard for AD and amnestic MCI respectively (American Psychological Association., 2000; Petersen, 2004). Controls were those that had some memory complaints but did not meet the standard of MCI or AD. AD patients had an

average Mini Mental State Examination (MMSE) score 23±2; control subjects had an average MMSE score 29±1 and MCI had an average score of 27±1.

B. PET scanning

A bolus of FDDNP (320 to 550 MBq) (Liu et al., 2007) was injected through an indwelling venous catheter and a dynamic PET scan performed for up to 125 minutes (six 30-second frames then four 180-second frames followed by five 600-second frames, finished with three 1200-second frames) using an ECAT EXACT HR+ scanner (Siemens Corp.). There was no head restraint for the patients, since head restraints could be very uncomfortable for the patients. Scans were corrected for decay and reconstructed with the use of a filtered back-projection algorithm (Hann filter; 0.3 of the Nyquist frequency with a zoom factor of 3.5) with attenuation correction factors calculated from transmission measurements (acquired for 20 min in 2D acquisition mode with the same PET scanner at ~10 min before the injection of FDDNP)). The resulting images had a resolution of 9 mm full width at half maximum (FWHM) and contained 63 contiguous slices with image plane separation of 2.42 mm.

C. MRI scanning

A whole-brain spoiled gradient echo MRI (MPRAGE) volumetric scan was taken for each individual with a 3T Siemens Allegra MRI scanner (sagittal plane; repetition time (TR) 2300 ms; echo time (TE) 2.93 ms; 160 slices; slice thickness 1 mm, skip 0.5 mm; in-plane voxel size 1.3 × 1.3 mm; field of view 256 × 256; flip angle 8°) (Thompson et al., 2004).

D. Cortical Surface Mapping

An affine transformation (composed of any linear transformation like rotation, scaling and shear plus translation that preserves collinearity) was performed on the MRI of each subject to put it first into the International Consortium for Brain Mapping (ICBM53) common space (Mazziotta et al., 2001). ICBM is a reference system for structural and functional anatomy of the brain. “Minctracc”, a program for elastic image registration (Collins et al., 1994), was used to map the MR images into the ICBM space. A 3D hemispheric cortical surface model for each subject was extracted from his/her MRI in the ICBM space as described by Thompson et al. (Thompson et al., 1997). The result was a triangular discrete model for the surface where the boundaries between gray matter and CSF are distinguished. To improve the MRI alignment among individuals, an elastic warping based on matching the sulci locations was performed in addition to the first mapping to bring the MR into ICBM space. Using the two mappings together brings each FDDNP cortical surface into the same space so that statistical analysis can be performed more robustly on the images. In the elastic warping, 36 major fissures and sulci were manually identified. For each hemisphere, some of the 3D sulcal curves drawn were the Sylvian fissure, superior, middle and inferior frontal, central, post-central, precentral, intraparietal, superior and inferior temporal, collateral, olfactory and occipito-temporal sulci, transverse occipital, primary intermediate, and secondary intermediate(Sowell et al., 2000; Thompson et al., 1997). This surface was flattened into a 2D plane where the sulcal curves drawn in 3D on the surface were re-identified. A RGB (Red Green Blue) flat color map to preserve the 3D locations was determined. For each individual, the sulcal pattern of that individual was nonlinearly aligned to an average sulcal pattern with an elastic transformation (Thompson et al., 2003; Thompson et al., 2004; Thompson et al., 2002). This additional alignment decreased the existing variability between individuals that might confound studies of large groups. This mapping was performed on the RGB map to bring back the newly aligned individual into a 3D cortical map.

E. Correction of Movement Artifacts

Dynamic FDDNP scans were corrected for head movement during the up-to–125 minutes-scan by first determining the proper attenuation of the emission (EM) frames, by aligning the transmission image to each EM frame. The emission data were re-reconstructed using the aligned transmission scan for attenuation correction. After that each corrected EM frame was aligned to a reference frame. The co-registration was done using SPM2 (Statistical Parametric Mapping, Institute of Neurology, University College of London, UK) software package (Frackowiak, 2004) and with the criterion of maximizing the normalized mutual information. This procedure has been described in detail (Wong, 2007b).

F. Preparation of DVR images

FDDNP DVR images were generated following the procedure described previously (Kepe et al., 2006; Small et al., 2006). Briefly, Logan graphical analysis (Logan et al., 1996) were applied to the dynamic FDDNP PET images using cerebellar region of interest (ROI) as the reference region to determine the DVR values of FDDNP in all brain tissue voxels. Cerebellar ROI was drawn on the cortical cerebellar region of the image that summed up the images from 0 to 6 minutes. The ROI was projected to all time frames of the dynamic images, and the time activity curve (TAC) corresponding to the cerebellar region was obtained. This cerebellar TAC was used as the input function in the Logan analysis of the dynamic image. The DVR value for each image voxel location was the linear slope of the Logan plot (Logan et al., 1996) for the corresponding image values between 15 and 125 minutes (Small et al., 2006).

G. Alignment of PET with MR Images

Using SPM2 (Frackowiak, 2004), the early summed (1–7 frames) FDDNP PET image was aligned to the MR image of the subject by rigid-body co-registration. Maximizing the normalized mutual information was the criterion used in the rigid-body registration. The early summed FDDNP image preserved the anatomical information needed for accurate co-registration to MRI. The FDDNP DVR image, which is in the same space as the early summed FDDNP image, was then warped to the right orientation by following the same transformations for the MRI. The affine mapping mentioned in subsection D to bring the MRI images into ICBM space was then applied to the co-registered early summed FDDNP images and the DVR PET image, so they were all in the same ICBM common space, and thus in the same cortical surface derived from the warped MRI.

H. Calculating PET values for the cortical surface map

The cortical surface model described in subsection D above was applied to the aligned and masked DVR PET image, giving a cortical surface map of FDDNP signal at each cortical surface vertex. The average DVR value within a sphere (excluding the extra-cerebral space) around each cortical point in the 3D FDDNP DVR PET image in ICBM space of a certain radius was calculated to give a DVR FDDNP value for that cortical point on the surface map. This radius of the sphere is referred to as the kernel size or cortical surface smoothing factor in the rest of the manuscript. The spherical kernel is like a kernel in a convolution operation except that in the present case the voxel values outside of the brain are not included in the calculation. The kernel size was varied from 7 mm to 17 mm to determine its effect on the values on the cortical surface map. In addition, ROI values obtained on the cortical surface as well as on the corresponding 3D DVR PET image were compared (see subsection below) to verify the quantitative nature of the values on the cortical surface map.

I. ROI analysis

Regional analyses, such as that described in the MarsBaR SPM software toolbox, have been used to study metabolic differences in defined brain regions among different subject groups

(Brett et al., 2002). In this study, a cortical surface ROI program written in MATLAB (version 6.5, The Mathworks Inc., Natick, MA 2002) was used to draw various surface ROIs (volume of interest) directly on the average cortical surface by picking all points on the cortex within a sphere of user defined radius. With this surface ROI tool, values in various regions on the cortical surface were examined. Nine anatomical ROIs in the frontal, temporal, parietal, and posterior cingulate gyrus were picked directly on the cortical surface. Each cortical surface ROI was also made into a 3D mask on the corresponding original PET image by selecting all voxels within a given radius (e.g., 7 mm) around each individual cortical point in the surface ROI. Based on this 3D mask, regional FDDNP DVR values on the original PET images corresponding to these surface ROIs were calculated. The average value obtained for each region on the cortical surface (i.e., from the cortical surface map) was compared with those directly obtained from the corresponding mask on the 3D FDDNP PET.

J. Partial Volume Correction

A simulated FDDNP PET image was created from a mask of the cerebral cortex derived from the MR image with gray and white matter regions both assigned a unit value (since the global FDDNP DVR value in gray: white is very close to 1:1)(Wong et al., 2007a; Wong et al., 2008). A second image was created by 3D smoothing of the simulated PET image (with a Gaussian kernel of FWHM=9 mm to simulate spatial resolution of the PET scanner). The mean value from a sphere, of fixed radius, around each cortical surface point was then determined for both the unsmoothed and the smoothed PET images so simulated. The partial volume correction factor (PVCF) for each surface point was then calculated by dividing the intensity for each cortical point of the unsmoothed PET image with the value from the corresponding points on the cortical map of the smoothed image. The intensity of the unsmoothed PET image is equal to 1.0 for each cortical point for each individual in this study. The partial volume corrected (PVC) surface map was obtained by multiplying the DVR values on the surface map with the PVCF of the corresponding surface points (Hoffman et al., 1979).

The use of different contrast levels between gray and white matter regions in PVC was also investigated. We found that increasing the gray-to-white contrast up to 1.4 increased the scaling, but did not affect the relative distribution/pattern of the PVC cortical surface images.

K. Discriminant Analysis

Discriminant analysis (Afifi et al., 2004) using SPSS (SPSS for Windows, Rel. 16.01. 2007. Chicago: SPSS INC.) was performed to classify the FDDNP cortical surfaces of the AD and control groups. This analysis requires prior knowledge of the groups in addition to the pattern of FDDNP intensity for categorization. Total ROI values for the six cortical surface ROIs previously mentioned (frontal (2), lateral temporal (2), medial temporal (1), parietal (1)) for each hemisphere were used for the discriminant analysis. Total ROI value for each ROI was calculated as the mean of the cortical surface values that were above 60% of the peak value within each ROI. Discriminant analysis was performed for all subsets of the 6 regions. Each subset of the six FDDNP DVR ROIs was put through discriminant analysis. To determine whether a model was appropriate, we examined four criteria, the canonical coefficients, Box M analysis, Wilke’s Lambda and classification and cross validation percentages. Box M Analysis was used to determine whether the covariance matrices differ between the groups. The cross validation percentages were calculated by removing one subject at a time from the study, determining the discriminant model from the new subgroup, and finally predicting the classification of the subject from this new model. The cross-validation results would indicate the robustness of the model. The cortical surface maps of all the individuals were then ordered according to their discriminant scores (calculated based on the discriminant function of a model).

L. Regression analysis

The cortical surface maps were also ordered according to the subjects' MMSE scores. Linear and polynomial regressions with a least-squares criterion were performed across all subjects in the studied group for FDDNP DVR value on each surface point versus the subjects' MMSE scores. F-statistic was used to test the significance of the regression coefficients (Neter, 1996).

III. Results

A. Effects of Movement Correction on FDDNP DVR cortical surfaces

As shown in Figure 1, head movement correction of the dynamic FDDNP PET images clearly improved the resulting FDDNP DVR images, particularly those of AD subjects, as reported earlier (Wong, 2007b). For this experiment, we were just looking at movement therefore we did not correct for PVE and the kernel size was 9 mm. The largest amount of head movement among the subjects studied consisted of a translation of >10 mm and a rotation of >9 degrees during the dynamic FDDNP PET scan. Cortical FDDNP surface maps that used the movement-corrected DVR images presented less left-right asymmetry. In addition, a decrease in intra-group variability (e.g., maximal coefficient of variation reduced from 0.2 to 0.16) was seen for cortical surface maps generated from DVR images with movement correction. There was an increase in the number of cortical points, from 10.2% to 26.2% of the cortex over both hemispheres that were significantly different with a threshold of $p<0.05$ between control and AD subjects. Increases in areas of significant difference between control and AD subjects in the various cortical regions were as follows: 26% in lateral temporal, 38% in parietal, 20% in frontal, 18% in posterior cingulate gyrus, but only 3% in medial temporal region. Using discriminant analysis, the classification was improved after movement correction. While there were 14 models that had a classification/cross-validation accuracy of at least 94.1%/82.4% or better, the non-movement corrected model had only 5 models with that percentage or higher.

B. Effects of Kernel size

Kernel size affected the cortical surface values as well as the group standard deviation maps (Figure 2A and B). For larger kernel sizes, the ranges of the surface DVR intensity in all three groups (AD, control and MCI), were smaller and the cortical surface images were smoother. The variability shown on the coefficient of variation maps for both control and AD patients generally decreases as kernel size increases (decreased by at least 50% as the kernel size increased to 17 mm).

The kernel size had noticeable effects on the separation of the average surface maps between AD group and normal controls. The FDDNP DVR values on each cortical surface point of the AD patients were compared with those of the normal controls on the same cortical surface location (t-test). A probability p for chance occurrence of the difference in mean values was calculated for each surface point. The p value cortical surface maps so generated are shown in Figure 2C for kernel sizes ranging from 7 to 17 mm. As kernel size was increased from 7 to 17 mm, most cortical areas showed significant difference between control and AD groups. Regions in the medial cortical surface (e.g., anterior and posterior cingulate gyruses and medial temporal lobes) were significantly different between AD and normal control groups even at a kernel size of 7 mm with increases in significant FDDNP DVR differences for larger kernel sizes. The mean and standard deviation values for two representative cortical surface ROIs (e.g., temporal and medial temporal regions) with various kernel sizes are shown in Table 1.

We compared the 3D surface ROIs with various kernel sizes with a common 3D volume of interest (VOI) method. For each region, each kernel size and each subject group, the FDDNP mean intensity on the cortical surface map was indistinguishable from the mean intensity

determined by the common VOI method ($p>0.05$; two sided t-test with unequal variances). However, the sum of squares of differences between the cortical ROI values and the VOI values of the corresponding regions on the original PET image is smallest for kernel size of 11 mm (0.127) over all VOIs in both hemispheres (18 regions). A kernel size of 9 mm provides only a slightly higher value (0.133). In the discriminant analysis, we found that there were 7 models with a classification/cross-validation accuracy of above 94.1%/82.4% using a 3D VOI method compared to 14 models for the cortical surface method with 9 mm and 7 models for a kernel size of 11 mm. The cortical surface method with a kernel size of 9 mm provided better classification than a common 3D VOI method probably due to a better inter-subject alignment of the cortical surface map with its sulci coregistration.

Judging by the results of discriminant analysis for classification between control and AD subjects, a kernel size of 9 mm was better than other kernel sizes (Table 2). There were 12 models with classification/cross-validation accuracy of above 94.1%/82.4% for kernel size of 7 mm, 14 models for kernel size of 9 mm, 7 models for kernel size of 11 mm, 3 models for kernel size of 13 mm, 1 model for kernel size of 15 mm, and 1 model for kernel size of 17 mm.

C. Partial Volume Correction of FDDNP cortical surface maps

Cortical surface FDDNP DVR map with PVC is shown in Figure 3A in comparison with the same map without PVC. Without PVC, DVR values on the medial surface were significantly higher than on the lateral surface. But with PVC, the DVR values on lateral and medial surfaces became comparable, which demonstrated the predictable ‘contaminant’ effect of neighboring affected areas, which occurs for all PET images. Partial volume correction also improved the separation of FDDNP DVR values in the medial surface between the control and AD groups (Figure 3B). Student’s t-test of DVR values between control and AD patients had a large increase in the significance level in the medial regions, particularly the anterior and posterior cingulate gyri, with little change in the significance level for the cortical lateral regions, as shown in Figure 3B. Applying discriminant analysis to both PVC PET and PET, we found that while, without PVC, there were only 14 models that had a classification/cross-validation accuracy of at least 94.1%/82.4% or better, PVC PET had 20 models with that accuracy or better.

D. Progression of FDDNP PET cortical map binding with MMSE scores

Progression of FDDNP DVR pattern with MMSE score is shown in Figure 4 by use of regression analysis. Increases in the FDDNP DVR signal were first observed in the medial temporal cortices, progressively moving towards lateral temporal and parietal cortices. With MMSE score clearly indicating AD symptoms (e.g., MMSE=24), FDDNP binding signal already reached the frontal cortex (Figure 4A). The FDDNP DVR signal on each cortical surface point (thus the cortical FDDNP DVR surface map) at any MMSE value in the range investigated (30 to 15) could be determined based on the regression line for each point on the cortical surface (Figure 4A). The slope determined from the linear regression model (Figure 4B) showed significantly higher rates of FDDNP signal increase in the lateral and medial temporal regions as well as in the anterior and posterior cingulate areas known to have high levels of Aβ and NFT in AD patients (Braak and Braak, 1991;Small et al., 2006). The data however did not support a second order polynomial model, based on a partial F-statistic test (Neter, 1996). The areas with a significant slope between FDDNP DVR intensity and MMSE score, particularly in the frontal, temporal, parietal, posterior cingulate, anterior cingulate and medial temporal regions, can be seen in Figure 4C.

E. Classification of FDDNP PET images using discriminant analysis

The discriminant analysis based on the ROI values obtained from the cortical FDDNP DVR surface map classified well the maps between control and AD groups. Obviously the selection

of subjects for this study was based on their various clinical diagnosis, but discriminant analysis is most importantly an excellent approach for ordering subject FDDNP surfaces to characterize disease progression. Figure 5B and 5C show the ordering of the cortical surface maps created according to the discriminant score that was based on cortical surface ROI values in the parietal (1), lateral temporal (6) and medial temporal regions (9). This particular discriminant analysis was performed on the left hemisphere for illustration of the method. The discriminant scores characterized the pattern for all subjects (Figure 5C). It clearly shows the increase in FDDNP binding starting from temporal and propagating to frontal and parietal areas. The ROI value in the medial temporal region had the highest weight (0.620) in the discriminant function. Based on a discriminant score threshold of 0.17 (provided by the discriminant analysis), the classification gave a sensitivity of 71% and specificity of 90% for separating ADs from normal controls. If the ROI values in both hemispheres were used, the classification gave a sensitivity of 86% and specificity of 100%.

IV. DISCUSSION

The brain cortical surface method described in this work for FDDNP demonstrated, in the living brain of human subjects, the gradual progression of cortical pathology deposition with AD progression. The FDDNP results are entirely consistent with known pathology of aggregate deposition obtained earlier with brain specimens (Braak and Braak, 1991, 1997). Equally important, the predictable progression of FDDNP provides a ‘fingerprint’ of progressive pathology deposition and provides an opportunity to classify patients for clinical diagnosis. Thus, the FDDNP cortical binding status may help determine whether a given FDDNP brain pattern is compatible with possible AD. There are other PET probes besides FDDNP that have been used to image neuropathology deposition in AD, but they present alternative characteristics. For example, PIB does not have the same progression pattern, and various explanations have been offered in the literature. PIB’s binding pattern is different from that of FDDNP and does not follow the progressive nature demonstrated by neuropathological evaluation of autopsy specimens(Braak and Braak, 1991). PIB accumulation as AD progresses (e.g., from controls, MCI to AD) follow a pattern that has been described as an ‘on and off’ pattern that is typically not found in pathology specimens (Kemppainen et al., 2007; Mintun et al., 2006). Moreover, PIB has signals in AD in most brain regions except medial temporal compared with control patients (Shin et al., 2008), but a significant number of controls do present positive PIB binding (Mintun et al., 2006) and also some AD subjects present negative PIB binding (Leinonen et al., 2008). One of the explanations for the difference may be attributed to the fact that PIB does not bind to NFTs while FDDNP does (Shin et al., 2008; Tolboom et al., 2009).

The methodological analysis presented in this work demonstrated the importance of movement correction, optimization of kernel size, and partial volume correction in data quantification. In a previous work, we only used a kernel of 7 mm without optimization, did not use partial volume correction or movement correction (Braskie et al., 2008).

Movement correction eliminated artifacts usually affecting regional DVR values. After movement correction of dynamic FDDNP determinations, DVR values appeared in general more left-right symmetrical on the cortical surface. Discriminant analysis based on the movement corrected images had better classification of AD subjects from the normal control and was more robust. However the movement correction method used in this study also has some limitations, such as inability to correct for intra-frame head movements. Work is on-going in our laboratory to examine these limitations to achieve further improvements, and will be addressed separately.

A parameter that is important to optimize for the cortical surface method is the kernel size of the spherical ROI used to calculate the FDDNP DVR values for each point on the cortical surface. With smaller size kernel, noise due to movement, for example, would be higher. However, a larger radius has a stronger smoothing effect that reduces variations between adjacent pixel values and thus inter-subject variability on each cortical surface point in each group. With a kernel size of 17 mm, a significant difference was observed between control and AD throughout most regions of the cortex including the motor strip, which is supposed to have low Aβ and NFT. However, this difference assessment has not considered the correlation of the neighboring cortical surface points. To choose the appropriate kernel size in this study, the following variables were analyzed: (1) comparison of the values obtained by a traditional VOI method against those values obtained by the cortical surface ROIs, and (2) Discriminant analysis on FDDNP DVR cortical surface ROIs for separation of AD group from normal controls. For the first step, the kernel size that gave ROI values closest to those of the VOI method was deemed more appropriate. With a kernel size of 9 mm (up to 11 mm), the quantitative ROI values from the two methods gave mean values that were closest for all ROIs. Using discriminant analysis, it was found that 9 mm kernel size had the best classification between AD and control groups. Combining the results from both tests, the appropriate kernel size should thus be 9 mm.

In addition, the use of MR cortical surface to map FDDNP DVR allowed correction for Partial Volume Effect (PVE), which is a common concern due to the limited spatial resolution of PET (Rousset et al., 1998). Co-registration and co-mapping of PET images (FDG and/or FDDNP) with MRI provided the opportunity to investigate and correct for PVE. PVE and correction methods have been studied in many biomedical imaging applications (Meltzer et al., 1990; Muller-Gartner et al., 1992; Rousset et al., 1998; Yang et al., 1996). Even though there are limitations to common PVC methods due to their inability to account for true image variations within each regional mask and their sensitivity to exact boundaries between regions, application of reliable PVC is important to reveal the underlying biological changes in tissue. In this study, correction was made directly on the 3D cortical surface by creating a simulated FDDNP PET image from the MR derived cortical surface without segmenting out separate regions for gray and white matter regions. Alternatively, PVC can also be performed voxel-by-voxel on the 3D PET image first and the PVC results mapped to the cortical surface. Though the results are not expected to be much different between the two alternatives, performing PVC directly on the cortical surface is computationally less intensive due to the fact that there are less cortical points than voxels, and is less noise sensitive since the averaging by the spherical kernel is done first before multiplying with the PVCF. PVC FDDNP DVR was found to be important as it increased the separation of the DVR values between control and AD groups in the medial cortical regions, particularly the posterior cingulate and anterior cingulate regions. Thus, PVC PET increased the signal to noise ratio in the medial region. In addition, the PVC FDDNP discriminant function was more robust than that without PVC. PVC PET had 20 models that had classification/cross-validation accuracy of 94.1%/82.4% or higher, while, without PVC, there were only 14 models that had that percentage or better.

The standardization of the cortical surface maps not only facilitates examination of FDDNP PET cortical surfaces among different subject groups, but helps to evaluate the correlation of the surface maps with other behavior variables(Braskie et al., 2008). Defining the ‘fingerprint’ pattern of FDDNP cortical binding provides a powerful tool to delineate pathology progression that appears in consistent agreement with clinical diagnosis and disease progression. Therefore, individual subjects with unknown diagnosis could be classified based on the fingerprint, similarly to what is currently done with clinical diagnosis of dementia using FDG (Silverman, 2004; Silverman et al., 2002). By applying regression analysis in the present work, we observed significant progression of FDDNP binding starting from the temporal and propagating to the frontal cortex as MMSE score decreased (Figure 4). The regions of highest slope of the

regression analysis match well those of significant Aβ and neurofibrillary tangles deposition as determined by previous autopsy studies of AD (Braak and Braak, 1991, 1997) that include the lateral temporal, lateral frontal, anterior cingulate, medial temporal and posterior cingulate regions. Efforts to simplify and to streamline the cortical surface mapping procedure to make it more practical for routine analysis are ongoing. The model developed in this study thus can potentially be used routinely to diagnose AD suspected subjects based on their FDDNP patterns with a greater specificity than the global ROI value (sensitivity=86%, specificity=80%).

V. Conclusion

Cortical surface mapping of FDDNP DVR values were shown to reveal clearly the characteristic patterns of FDDNP binding after optimization of the signal by movement correction, kernel size, and partial volume correction. Movement correction and partial volume correction remove image artifacts that can obscure the binding pattern. Optimization of the kernel size allows closer correspondence between surface ROIs and a common VOI method. Characterization of a fingerprint of progression of FDDNP distribution shown in this study would permit in living subjects more precise diagnostic classification and establish whether individual patients fall into a pattern consistent with AD or should be classified under other dementias.

Acknowledgments

This research was funded by DOE contract DE-FC03-87-ER60615, NIH grants P01-AG025831, AG13308, P50 AG 16570, MH/AG58156, MH52453; AG10123; M01-RR00865, General Clinical Research Centers Program, the Fran and Ray Stark Foundation Fund for Alzheimer's Disease Research; the Ahmanson Foundation; and the Larry L. Hillblom Foundation. JRB gratefully acknowledges the support of the Elizabeth and Thomas Chair Endowment in Gerontology. No company provided support of any kind for this study. We would like to thank Dr. Jie Liu, Dr. Nagichettiar Satyamurthy and all at the UCLA Cyclotron, for synthesizing FDDNP. We also thank Mirwais Wardak, Dr. Koon-Pong Wong, and Weber Shao for their help with movement correction of PET images.

References

Afifi, AA.; Clark, V.; May, S. Computer-aided multivariate analysis. Vol. 4. Chapman & Hall/CRC; Boca Raton, Fla: 2004.

Agdeppa ED, Kepe V, Liu J, Flores-Torres S, Satyamurthy N, Petric A, Cole GM, Small GW, Huang SC, Barrio JR. Binding characteristics of radiofluorinated 6-dialkylamino-2-naphthylethylidene derivatives as positron emission tomography imaging probes for beta-amyloid plaques in Alzheimer's disease. J Neurosci 2001;21:RC189. [PubMed: 11734604]

American Psychological Association. Diagnosis and Statistical Manual of Mental Disorders DSM-IV-TR (Text Revision). Washington DC: 2000.

Braak H, Braak E. Neuropathological stageing of Alzheimer-related changes. Acta Neuropathol 1991;82:239–259. [PubMed: 1759558]

Braak H, Braak E. Frequency of stages of Alzheimer-related lesions in different age categories. Neurobiol Aging 1997;18:351–357. [PubMed: 9330961]

Braskie MN, Klunder AD, Hayashi KM, Protas H, Kepe V, Miller KJ, Huang SC, Barrio JR, Ercoli LM, Siddarth P, Satyamurthy N, Liu J, Toga AW, Bookheimer SY, Small GW, Thompson PM. Plaque and tangle imaging and cognition in normal aging and Alzheimer's disease. Neurobiol Aging. 2008

Brett, M.; Anton, J-L.; Valabregue, R.; Poline, JB. Region of interest analysis using an SPM toolbox [abstract]. Presented at the 8th International Conference on Functional Mapping of the Human Brain; June 2–6, 2002; Sendai, Japan. 2002. Available on CD-ROM in NeuroImage

Collins DL, Neelin P, Peters TM, Evans AC. Automatic 3D intersubject registration of MR volumetric data in standardized Talairach space. J Comput Assist Tomogr 1994;18:192–205. [PubMed: 8126267]

Fischl B, Dale AM. Measuring the thickness of the human cerebral cortex from magnetic resonance images. Proc Natl Acad Sci U S A 2000;97:11050–11055. [PubMed: 10984517]

Frackowiak, RSJ. Human brain function. Vol. 2. Academic Press; San Diego, Calif: 2004.

Guo Z, Zhang J. Experimental and Clinical study of Alzheimer disease on positron emission tomography: Imaging of beta-amyloi plaques. J Nucl Med 2007;48:256.

Hoffman EJ, Huang SC, Phelps ME. Quantitation in positron emission computed tomography: 1. Effect of object size. J Comput Assist Tomogr 1979;3:299–308. [PubMed: 438372]

Kemppainen NM, Aalto S, Wilson IA, Nagren K, Helin S, Bruck A, Oikonen V, Kailajarvi M, Scheinin M, Viitanen M, Parkkola R, Rinne JO. PET amyloid ligand [11C]PIB uptake is increased in mild cognitive impairment. Neurology 2007;68:1603–1606. [PubMed: 17485647]

Kepe V, Huang SC, Small GW, Satyamurthy N, Barrio JR. Visualizing pathology deposits in the living brain of patients with Alzheimer's disease. Methods Enzymol 2006;412:144–160. [PubMed: 17046657]

Leinonen V, Alafuzoff I, Aalto S, Suotunen T, Savolainen S, Nagren K, Tapiola T, Pirttila T, Rinne J, Jaaskelainen JE, Soininen H, Rinne JO. Assessment of beta-amyloid in a frontal cortical brain biopsy specimen and by positron emission tomography with carbon 11-labeled Pittsburgh Compound B. Arch Neurol 2008;65:1304–1309. [PubMed: 18695050]

Liu J, Kepe V, Zabjek A, Petric A, Padgett HC, Satyamurthy N, Barrio JR. High-yield, automated radiosynthesis of 2-(1-{6-[(2-[18F]fluoroethyl)(methyl)amino]-2-naphthyl}ethylidene) malononitrile ([18F]FDDNP) ready for animal or human administration. Mol Imaging Biol 2007;9:6–16. [PubMed: 17051324]

Loats, HL.; Holcomb, HH.; Loats, SE.; Tamminga, C. Cortical surface metabolic mapping. The Third International Peace through Mind/Brain Science Conference; Hamamtsu, Japan. August 5–10; 1990.

Logan J, Fowler JS, Volkow ND, Wang GJ, Ding YS, Alexoff DL. Distribution volume ratios without blood sampling from graphical analysis of PET data. J Cereb Blood Flow Metab 1996;16:834–840. [PubMed: 8784228]

Mazziotta J, Toga A, Evans A, Fox P, Lancaster J, Zilles K, Woods R, Paus T, Simpson G, Pike B, Holmes C, Collins L, Thompson P, MacDonald D, Iacoboni M, Schormann T, Amunts K, Palomero-Gallagher N, Geyer S, Parsons L, Narr K, Kabani N, Le Goualher G, Boomsma D, Cannon T, Kawashima R, Mazoyer B. A probabilistic atlas and reference system for the human brain: International Consortium for Brain Mapping (ICBM). Philos Trans R Soc Lond B Biol Sci 2001;356:1293–1322. [PubMed: 11545704]

Meltzer CC, Leal JP, Mayberg HS, Wagner HN Jr, Frost JJ. Correction of PET data for partial volume effects in human cerebral cortex by MR imaging. J Comput Assist Tomogr 1990;14:561–570. [PubMed: 2370355]

Mintun MA, Larossa GN, Sheline YI, Dence CS, Lee SY, Mach RH, Klunk WE, Mathis CA, DeKosky ST, Morris JC. [11C]PIB in a nondemented population: potential antecedent marker of Alzheimer disease. Neurology 2006;67:446–452. [PubMed: 16894106]

Muller-Gartner HW, Links JM, Prince JL, Bryan RN, McVeigh E, Leal JP, Davatzikos C, Frost JJ. Measurement of radiotracer concentration in brain gray matter using positron emission tomography: MRI-based correction for partial volume effects. J Cereb Blood Flow Metab 1992;12:571–583. [PubMed: 1618936]

Neter, J. Applied linear statistical models. Vol. 4. Irwin; Chicago: 1996.

Park HJ, Lee JD, Chun JW, Seok JH, Yun M, Oh MK, Kim JJ. Cortical surface-based analysis of 18F-FDG PET: measured metabolic abnormalities in schizophrenia are affected by cortical structural abnormalities. Neuroimage 2006;31:1434–1444. [PubMed: 16540349]

Petersen RC. Mild cognitive impairment as a diagnostic entity. J Intern Med 2004;256:183–194. [PubMed: 15324362]

Protas, HD.; Thompson, PM.; Hayashi, KM.; Yu, CL.; Bergsneider, M.; Huang, SC. Regional Quantitative Analysis of Cortical Surface Maps of FDG PET images. 2005 Nuclear Science Symposium and Medical Imaging Conference (NSS-MIC), Wyndham El Conquistador Resort; Puerto Rico. Oct. 23–29; 2005. MIC Conference Record IEEE

Rasser PE, Johnston P, Lagopoulos J, Ward PB, Schall U, Thienel R, Bender S, Toga AW, Thompson PM. Functional MRI BOLD response to Tower of London performance of first-episode schizophrenia patients using cortical pattern matching. Neuroimage 2005;26:941–951. [PubMed: 15955504]

Rousset OG, Ma Y, Evans AC. Correction for partial volume effects in PET: principle and validation. J Nucl Med 1998;39:904–911. [PubMed: 9591599]

Shin J, Lee SY, Kim SH, Kim YB, Cho SJ. Multitracer PET imaging of amyloid plaques and neurofibrillary tangles in Alzheimer's disease. Neuroimage 2008;43:236–244. [PubMed: 18694837]

Silverman DH. Brain 18F-FDG PET in the diagnosis of neurodegenerative dementias: comparison with perfusion SPECT and with clinical evaluations lacking nuclear imaging. J Nucl Med 2004;45:594–607. [PubMed: 15073255]

Silverman DH, Gambhir SS, Huang HW, Schwimmer J, Kim S, Small GW, Chodosh J, Czernin J, Phelps ME. Evaluating early dementia with and without assessment of regional cerebral metabolism by PET: a comparison of predicted costs and benefits. J Nucl Med 2002;43:253–266. [PubMed: 11850493]

Small GW, Kepe V, Ercoli LM, Siddarth P, Bookheimer SY, Miller KJ, Lavretsky H, Burggren AC, Cole GM, Vinters HV, Thompson PM, Huang SC, Satyamurthy N, Phelps ME, Barrio JR. PET of brain amyloid and tau in mild cognitive impairment. N Engl J Med 2006;355:2652–2663. [PubMed: 17182990]

Sowell, ER.; Thompson, PM.; Mega, MS.; Zoumalan, CI.; Lindshield, CJ.; Rex, DE. Gyral pattern delineation in 3D: surface curve protocol. 2000. www.loni.ucla.edu/~esowell/new_sulcvar.html

Thompson PM, Hayashi KM, de Zubicaray G, Janke AL, Rose SE, Semple J, Herman D, Hong MS, Dittmer SS, Doddrell DM, Toga AW. Dynamics of gray matter loss in Alzheimer's disease. J Neurosci 2003;23:994–1005. [PubMed: 12574429]

Thompson PM, Hayashi KM, Sowell ER, Gogtay N, Giedd JN, Rapoport JL, de Zubicaray GI, Janke AL, Rose SE, Semple J, Doddrell DM, Wang Y, van Erp TG, Cannon TD, Toga AW. Mapping cortical change in Alzheimer's disease, brain development, and schizophrenia. Neuroimage 2004;23 (Suppl 1):S2–18. [PubMed: 15501091]

Thompson PM, MacDonald D, Mega MS, Holmes CJ, Evans AC, Toga AW. Detection and mapping of abnormal brain structure with a probabilistic atlas of cortical surfaces. J Comput Assist Tomogr 1997;21:567–581. [PubMed: 9216760]

Thompson, PM.; Mega, MS.; Toga, AW. Subpopulation Brain Atlases. In: Toga, AW.; Mazziotta, JC., editors. Brain Mapping: The Methods. Academic Press; Amsterdam: 2002.

Tolboom N, Yaqub M, van der Flier WM, Boellaard R, Luurtsema G, Windhorst AD, Barkhof F, Scheltens P, Lammertsma AA, van Berckel BN. Detection of Alzheimer Pathology In Vivo Using Both 11C-PIB and 18F-FDDNP PET. J Nucl Med. 2009

Van Essen DC, Drury HA. Structural and functional analyses of human cerebral cortex using a surface-based atlas. J Neurosci 1997;17:7079–7102. [PubMed: 9278543]

Wong K, Kepe V, Small G, Satyamurthy N, Barrio J, Huang SC. Comparison of simplified methods for quantitative analysis of [18F]FDDNP PET data. Nuclear Science Symposium Conference Record, 2007, NSS'07, IEEE 2007a;4:3146–3150.

Wong K, Wardak M, Shao W, Dahlbom M, Kepe V, Liu J, Satyamurthy N, Small GW, Barrio JR, Huang SC. Quantitative Analysis of [18F]FDDNP PET using Subcortical White Matter as Reference Region. J Nucl Med 2008;49:117P.

Wong KP, Wardak M, Shao W, Zhou Z, Dahlbom M, Smid L, Truong D, Kepe V, Small GW. Movement correction of [18F]FDDNP PET studies for brain amyloid. Nuclear Science Symposium Conference Record, 2007, NSS'07, IEEE 2007b;5:3974–3977.

Yang J, Huang SC, Mega M, Lin KP, Toga AW, Small GW, Phelps ME. Investigation of Partial Volume Correction Methods for Brain FDG PET Studies. IEEE Transactions on Nuclear Science 1996;43:3322–3327.

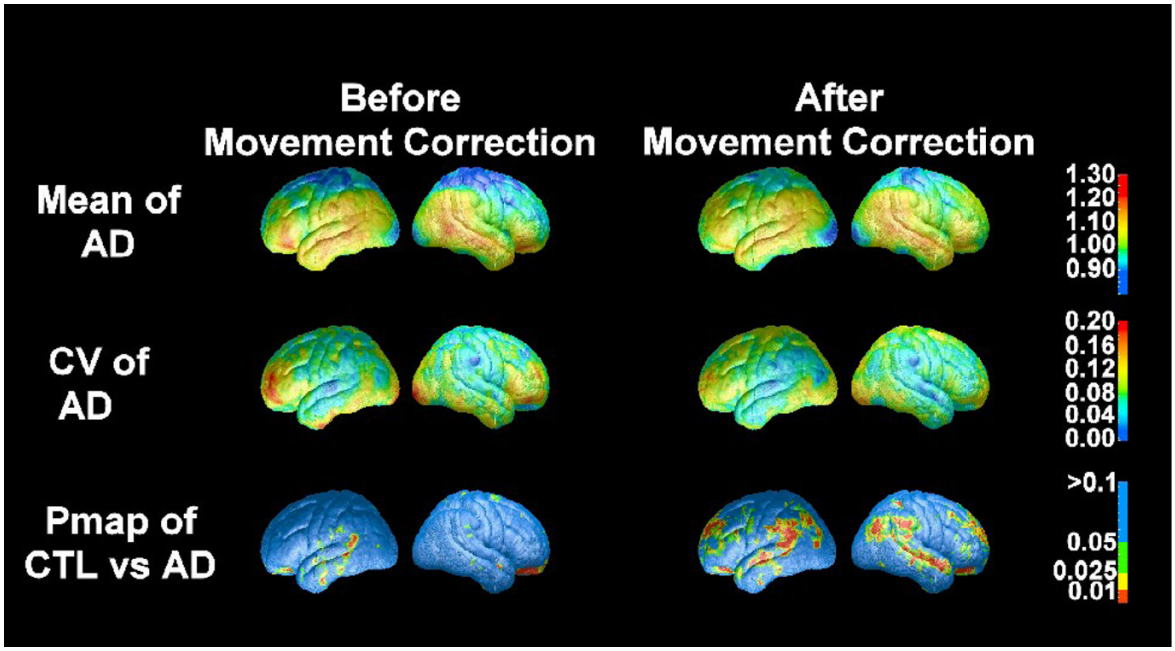

Fig. 1.

The average and coefficient of variation (CV) FDDNP DVR cortical surface map for the AD group (n=7) can be seen before and after movement correction. In addition, the pmap for a t-test performed between the AD and control groups (n=10) is shown in the bottom row, before and after movement correction.

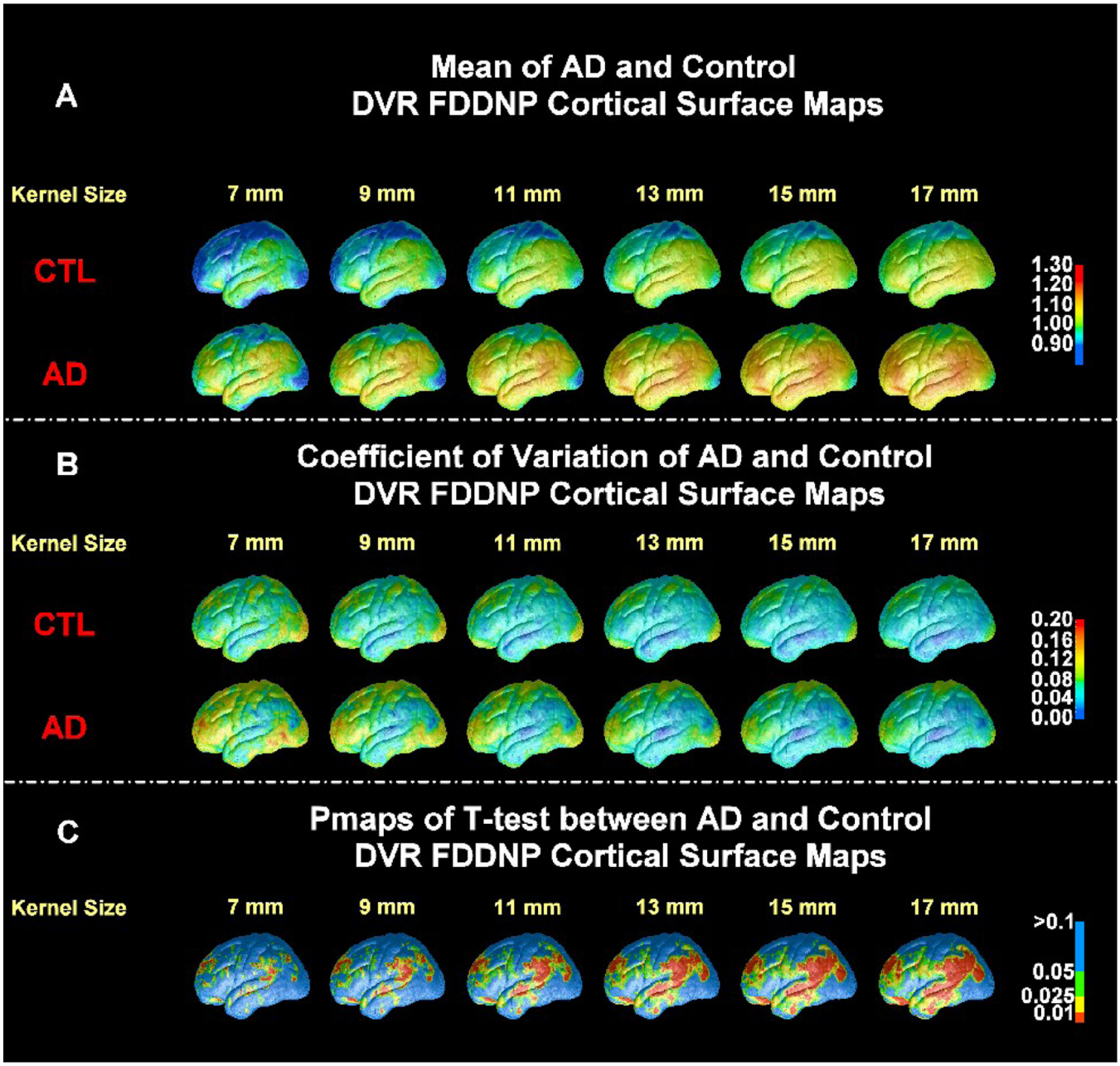

Fig. 2.

A. Average Cortical surfaces with FDDNP PET of AD patients and control subjects with different kernel sizes from 7 mm radius on the left until 17 mm radius on the right. A different pattern emerges depending on the kernel size. B. Effect of kernel size on cortical maps of standard deviation of FDDNP. Decrease in variability can be seen as kernel size increases. C. Effect of kernel size on cortical maps of p value determined from t-test for each cortical point between FDDNP in AD patients and control patients. An increase in the area of significance can be seen as p value increases.

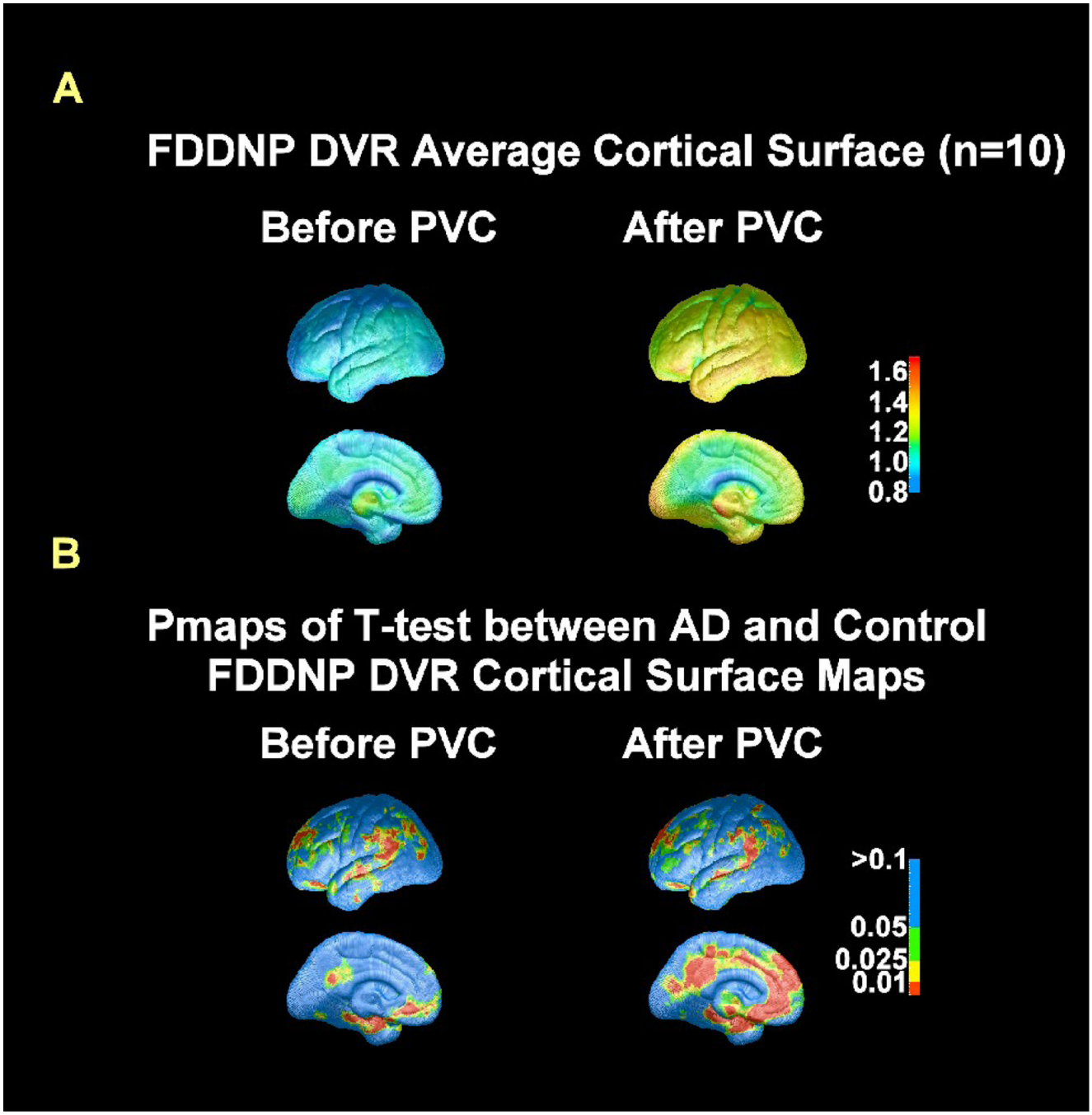

Fig. 3.

A. Cortical surface maps are shown for the average of 10 control subjects with FDDNP PET information before PVC (left) and after PVC (right). The pattern of FDDNP on the lateral cortical surface shows minimal changes in relative distribution between images with and without PVC in spite of the scaling differences. However, a large signal change was seen between the medial and lateral cortical surfaces with PVC compared to without PVC. B. Cortical surface map, containing the significance of t-test between 10 control subjects and 7 AD subjects before PVC (left) and after PVC (right), are shown. The pattern of the significance level on the lateral cortical surface at the top shows little difference between images with and

without PVC. However, an increase in the region with significant difference was seen on the medial surface.

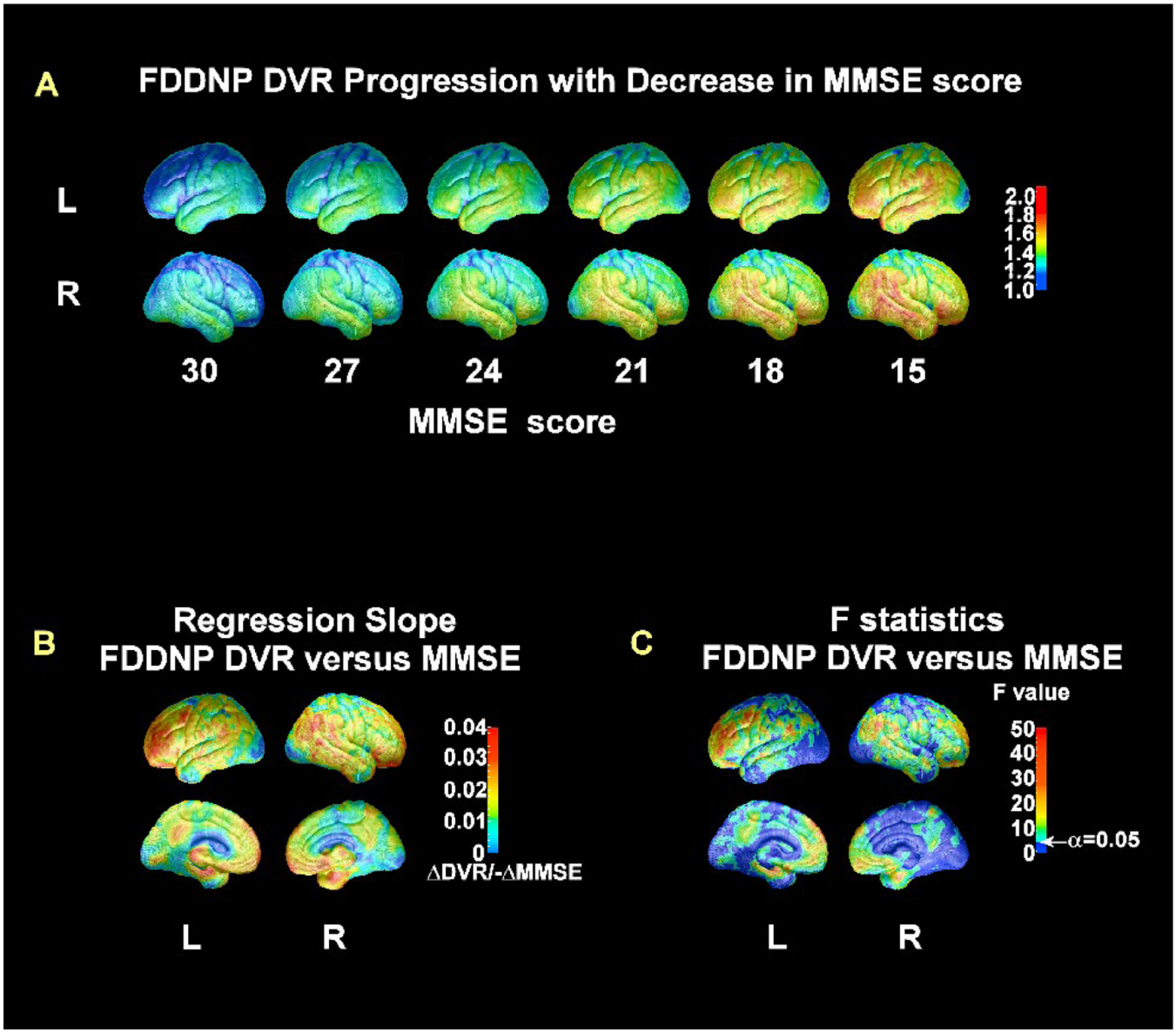

Fig. 4.

Panel A shows a hemispheric surface map of FDDNP DVR progression/spread as mini-mental state examination (MMSE) scores decreases. We see a similar trend between the left side and the right side. There is a bit of signal in the left temporal lobe at a normal MMSE of 30 that increases in the temporal lobe and spreads to the parietal and frontal areas as MMSE drops. This DVR spreading mimics the pathology progression of beta-amyloid plaques and neurofibrillary tangles accumulation in Alzheimer's disease. Panel B shows the surface map of regression slope of FDDNP DVR increase per unit change of MMSE score. The higher the slope corresponds to a faster increase of the FDDNP DVR. The areas of highest slope (red) match areas of significant beta-amyloid plaques and neurofibrillary tangles in AD that include the lateral temporal, lateral frontal, anterior cingulate, medial temporal and posterior cingulate areas. Panel C showsa cortical surface map of F statistics of the linear regression model between PVC FDDNP DVR and MMSE. Areas that have a significant slope with α=0.05 are shown with colors above dark blue. It is important to note that lateral frontal, lateral temporal, medial

temporal, anterior cingulate and posterior cingulate all have a significant slope, and all have been shown to be important in AD.

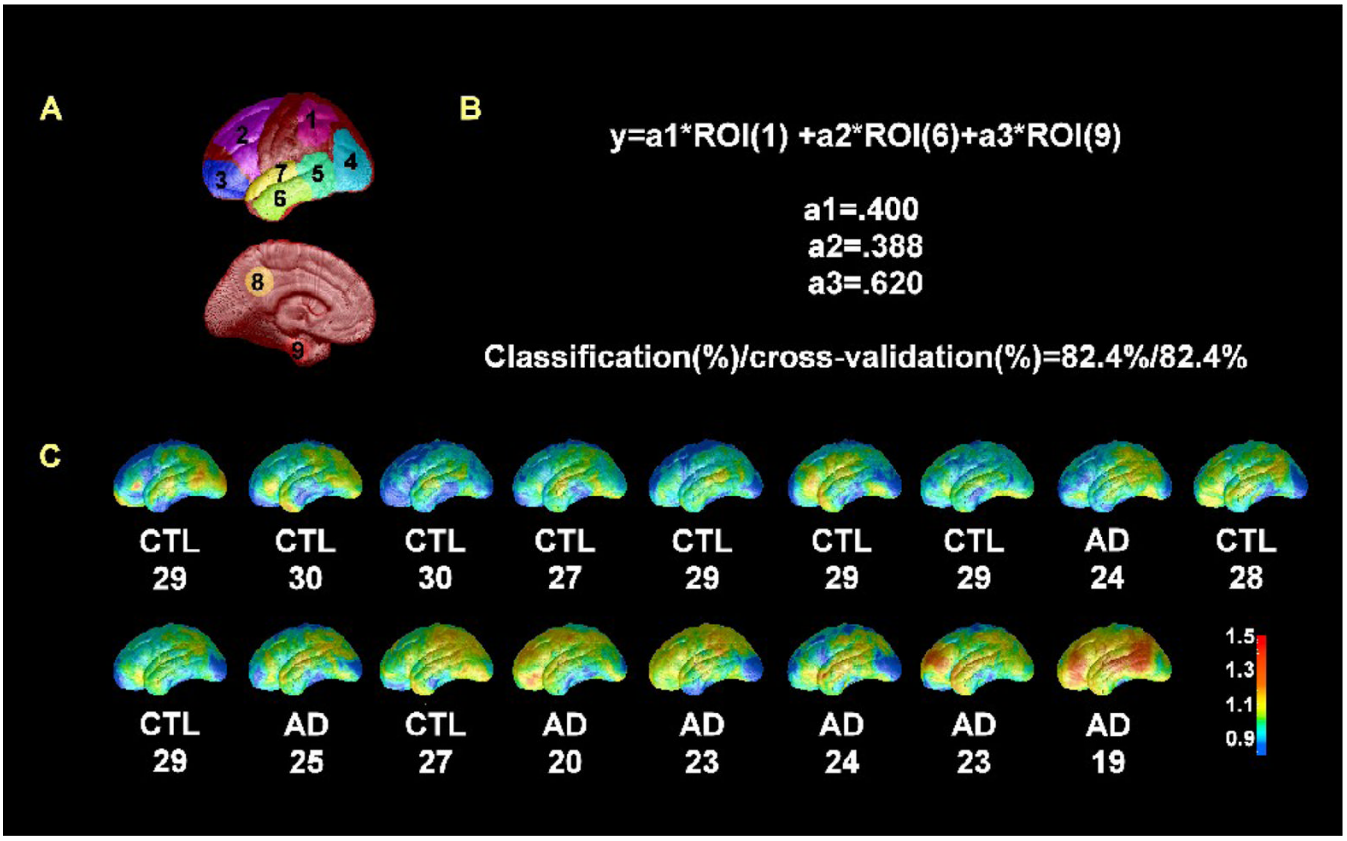

Fig. 5.

Panel A shows the cortical ROIs used in the lateral and medial cortex shown on the left hemisphere for discriminant analysis. Panel B shows the Standardized Canonical Discriminant Coefficients for a model including the parietal region (1), temporal region (6), and medial temporal region (9). The largest coefficient in the determination of the discriminant score is for the medial temporal region. Panel C shows the ordering of the cortical surfaces with respect to discriminant score based on the model in (B). The clinical diagnosis and MMSE score can be seen below each cortical surface map. The cortical surface is shifted so one can see a little of medial temporal region without obstructing the lateral side.

Table 1

DVR values in 2 cortical surface ROIs for both ROI method and for the cortical surface method with a kernel size of 7 mm, 9 mm, 11 mm, 13 mm, 15 mm, 17 mm

		Temporal cortex		Medial temporal cortex	
		CTL	AD	CTL	AD
VOI method[†]		0.999±0.027**	1.057±0.040	0.950±0.053**	1.044±0.044
	7 mm	0.958±0.032	1.007±0.052	0.941±0.035**	1.024±0.041
	9 mm	0.985±0.030*	1.039±0.045	0.956±0.042**	1.051±0.040
Kernel size	11 mm	1.005±0.029**	1.063±0.040	0.976±0.045**	1.071±0.039
	13 mm	1.020±0.028**	1.081±0.036	0.991±0.045**	1.085±0.039
	15 mm	1.032±0.028**	1.095±0.033	1.004±0.044**	1.095±0.039
	17 mm	1.041±0.029**	1.104±0.031	1.014±0.043**	1.101±0.039

** There is a significant difference between the reference group (AD group) and the test groups (control group) at a p=0.01 for the ROI in question using a two tailed t-test with unequal variance.

* There is a significant difference between the reference group (AD group) and the test groups (control group) at a p=0.05 for the ROI in question using a two tailed t-test with unequal variance.

† Using a two tailed t-test with unequal variances at a p=0.05 there are no significant differences for both AD and control between the VOI method and the cortical surface method for a kernel size of 7 mm, 9mm, 11 mm, 13 mm for medial temporal ROI. For a temporal region, there are no differences between a VOI method and a cortical surface method with a kernel size of 9 mm, 11 mm, 13 mm for a tempora1 region in a control group, while for the same ROI there are no differences in the AD group between a VOI method and a cortical surface method with kernel size of 7 mm, 9 mm, 11 mm, 13 mm, 15 mm.

Table 2

Discriminant Analysis Classification and Cross-validation Percentages for Various Models with Kernel Size Ranging from 7 mm–17 mm

Kernel Model	7 mm	9 mm	11 mm	13 mm	15 mm	17 mm
6,9*	94.1%/82.4%	88.2%/88.2%	88.2%/88.2%	82.4%/82.4%	82.4%/82.4%	82.4%/82.4%
1,2,9	94.1%/88.2%	94.1%/82.4%	88.2%/82.4%	88.2%/82.4%	88.2%/82.4%	88.2%/76.5%
1,6,9	88.2%/76.5%	94.1%/82.4%	88.2%/76.5%	82.4%/76.5%	82.4%/76.5%	82.4%/76.5%
2,6,9	94.1%/76.5%	88.2%/88.2%	88.2%/88.2%	88.2%/82.4%	82.4%/82.4%	82.4%/82.4%
3,6,9	94.1%/88.2%	88.2%/82.4%	88.2%/82.4%	82.4%/76.5%	82.4%/76.5%	82.4%/76.5%
2,7,9	88.2%/76.5%	94.1%/88.2%	94.1%/94.1%	94.1%/88.2%	94.1%/82.4%	94.1%/82.4%
6,8,9	94.1%/82.4%	88.2%/88.2%	88.2%/82.4%	94.1%/76.5%	94.1%/76.5%	94.1%/76.5%
1,2,6,9	94.1%/94.1%	94.1%/82.4%	88.2%/76.5%	88.2%/76.5%	88.2%/76.5%	88.2%/76.5%
2,6,7,9	94.1%/76.5%	94.1%/88.2%	94.1%/88.2%	94.1%/82.4%	94.1%/76.5%	88.2%/76.5%
2,3,6,9	94.1%/82.4%	88.2%/82.4%	88.2%/82.4%	82.4%/76.5%	82.4%/76.5%	82.4%/76.5%
1,2,6,7,9	94.1%/82.4%	94.1%/88.2%	94.1%/82.4%	88.2%/76.5%	88.2%/76.5%	82.4%/70.6%
2,3,6,7,9	94.1%/76.5%	94.1%/82.4%	94.1%/82.4%	94.1%/76.5%	88.2%/76.5%	88.2%/76.5%

* ROIs included in the model 1:parietal, 2: frontal, 3: prefrontal, 6: inferior temporal, 7:superior temporal, 8: posterior cingulate, 9: medial temporal ROI.